Editors' Suggestion | Featured in Physics

New Constraints on Axion-Mediated Spin Interactions Using Magnetic Amplification

Haowen Su,[1,2] Min Jiang,[1,2,*] Yuanhong Wang,[1,2] Ying Huang,[1,2] Xiang Kang,[1,2] Wei Ji,[3,4] Xinhua Peng,[1,2,†] and Dmitry Budker[3,4,5]

[1]CAS Key Laboratory of Microscale Magnetic Resonance and School of Physical Sciences, University of Science and Technology of China, Hefei, Anhui 230026, China

[2]CAS Center for Excellence in Quantum Information and Quantum Physics, University of Science and Technology of China, Hefei, Anhui 230026, China

[3]Helmholtz-Institut, GSI Helmholtzzentrum für Schwerionenforschung, Mainz 55128, Germany

[4]Johannes Gutenberg University, Mainz 55128, Germany

[5]Department of Physics, University of California, Berkeley, California 94720-7300, USA

(Received 13 November 2023; revised 6 June 2024; accepted 12 August 2024; published 4 November 2024)

Axions are highly motivated hypothetical particles beyond the standard model that can be dark matter candidates and address the strong *CP* problem. Here we search for axion-mediated interactions generated between two separated ^{129}Xe gas ensembles, monitoring and polarizing the ^{129}Xe nuclear spins through spin-exchange interactions with Rb vapor. Our method exploits the magnetic amplification through effective fields from Rb-Xe collisions, increasing the sensitivity for axion-mediated interactions by up to 145-fold relative to conventional methods. Moreover, we employ template filtering to extract exotic interactions with a maximum signal-to-noise ratio. By combining two techniques, axion-mediated interactions are constrained to be less than 10^{-5} of normal magnetic interactions on a length scale of 60 mm. We establish new constraints on the neutron-neutron pseudoscalar couplings for a mass range that expands into the well-motivated "axion window" (10 μeV–1 meV), improving previous constraints by up to 50-fold within it and 118-fold outside it. We further discuss promising applications in searches for other axion-nucleon interactions, including axion dark matter and black hole axion bursts with sensitivity well beyond astrophysical limits by several orders of magnitude.

DOI: 10.1103/PhysRevLett.133.191801

Introduction—Axion and axionlike particles predicted by numerous theories embed the standard model of particle physics into a more general, unified framework [1–8]. The main challenge encountered in the search for axions stems from their wide-ranging mass. Several theories (e.g., high-temperature lattice QCD [9], the standard model axion seesaw Higgs portal inflation model [10], and axion-string networks [11–15]) propose the axion window (10 μeV–1 meV) as one of the most likely regions of parameter space where axions may exist. Previous constraints from laboratory searches (e.g., ADMX) and astrophysical observations (e.g., SN1987A) mostly explored mass ranges outside the window [16,17,17,18,18–25]. Recently, this mass range has been explored in both haloscope and "fifth-force" experiments, while other experiments are in preparation. The haloscope experiments include HAYSTAC [26], CERN axion solar telescope [27], ORGAN [28,29], MADMAX [30], and the Orpheus experiment [31]. Fifth-force experiments include ARIADNE [32] and SAPPHIRE [25].

Axions are predicted to mediate exotic interactions by a variety of theories beyond the standard model [1,2,33–36]. The basic experimental scheme to search for exotic interactions is to employ a sensitive detector of torques or forces on particles from a source on a certain length scale [13,20,32,37–53]. Searches for axion-mediated interactions have the advantage of covering many orders of magnitude in the axion mass, including the axion window, without scanning. Specifically, the pseudoscalar coupling to spin-polarized fermions is of particular theoretical interest because it is predicted by numerous theories with a broken high-energy symmetry [54] and is similar to the propagating torsion field predicted by several extensions of general relativity [55]. However, normal (i.e., standard model) magnetic interactions hinder searching for the exotic interactions. Previous experiments, respectively, constrained exotic interactions mediated by light axions (<1 μeV) to be less than 10^{-5} and 10^{-8} of their normal magnetic interactions on the length scale of 400 and 500 mm between two polarized neutron ensembles [20,21]. The constraints fall off exponentially with increasing axion mass and thus become less stringent within the axion window. A pioneering experiment by Ramsey [56] constrained the exotic interactions in this range to be less than 10^{-3} of normal

*Contact author: dxjm@ustc.edu.cn

†Contact author: xhpeng@ustc.edu.cn

 © 2024 American Physical Society

magnetic interactions. Therefore, it is imperative to develop novel techniques in searches for exotic spin-dependent interactions.

In this Letter, we demonstrate magnetic amplification to search for exotic spin-dependent interactions between two separated ^{129}Xe spin ensembles that are mediated by axions within the axion window. Tailoring a spin-monitoring technique assisted by an *in situ* ^{87}Rb magnetometer, our technique demonstrates remarkable amplification for pseudomagnetic fields induced by the exotic interactions by up to 145-fold. Through the combination of the template filtering and high sensitive spin-monitoring technique, our Letter maximizes the signal-to-noise ratio to extract the sought-after signal from exotic interactions. As a first application, we constrain the exotic interactions between polarized ^{129}Xe spins to be less than 10^{-5} of normal magnetic interactions on a length scale of 60 mm. New constraints on neutron-neutron spin coupling are placed in the mass range (3.2–24.3 μeV) expanding into the axion window and improve previous experimental constraints by up to 50-fold within the window and 118-fold outside it. Although demonstrated for the exotic spin-dependent interactions, the magnetic amplification can be applied to various axion-nucleon interactions, including axion dark matter and axion bursts from astrophysical events [57,58]. With current experiments, the sensitivity should exceed astrophysical limits [59,60] by several orders of magnitude.

Axion-mediated spin-dependent interactions—The setup contains two cells: a spin-sensor cell I with 0.026 amg ^{129}Xe, 0.33 amg N_2, and a droplet of ^{87}Rb; and a spin-source cell II with 3 amg ^{129}Xe, 0.066 amg N_2 buffer gas, and a droplet of ^{87}Rb metal. Each cell is shielded by a magnetic shield and placed within a five-layer magnetic shield, as shown in Fig. 1(a). The centers of the two cells are ≈60.5 mm apart from each other. In each cell, ^{87}Rb spins are polarized using a circularly polarized beam of 795 nm D1 light and ^{129}Xe spins are polarized via spin-exchange collisions with polarized ^{87}Rb spins [16,61,62]. The fractional contribution of neutrons in ^{129}Xe spins is 0.73 [63]. The axion-mediated interactions between polarized neutrons are ($c = \hbar = 1$) [34–36]

$$V_{\text{ps-ps}} = \frac{g_{\text{ps}}^n g_{\text{ps}}^n}{16\pi m_n m_n}\left[\hat{\boldsymbol{\sigma}}_{\text{I}}\cdot\hat{\boldsymbol{\sigma}}_{\text{II}}\left(\frac{m_a}{r^2}+\frac{1}{r^3}\right) - (\hat{\boldsymbol{\sigma}}_{\text{I}}\cdot\hat{r})(\hat{\boldsymbol{\sigma}}_{\text{II}}\cdot\hat{r})\left(\frac{m_a^2}{r}+\frac{3m_a}{r^2}+\frac{3}{r^3}\right)\right]e^{-m_a r}, \quad (1)$$

where g_{ps}^n is the neutron pseudoscalar coupling constant, m_n is the neutron mass, m_a is the axion mass, the spin vector $\hat{\boldsymbol{\sigma}}_{\text{I,II}}$ is labeled with subscript I for sensor and II for source (the same for other parameters), and r ($\hat{r}$) is the distance (unit vector) between the two interacting neutrons. The pseudomagnetic fields $\mathbf{B}_p$ experienced by the nuclei in the sensor cell can be deduced from

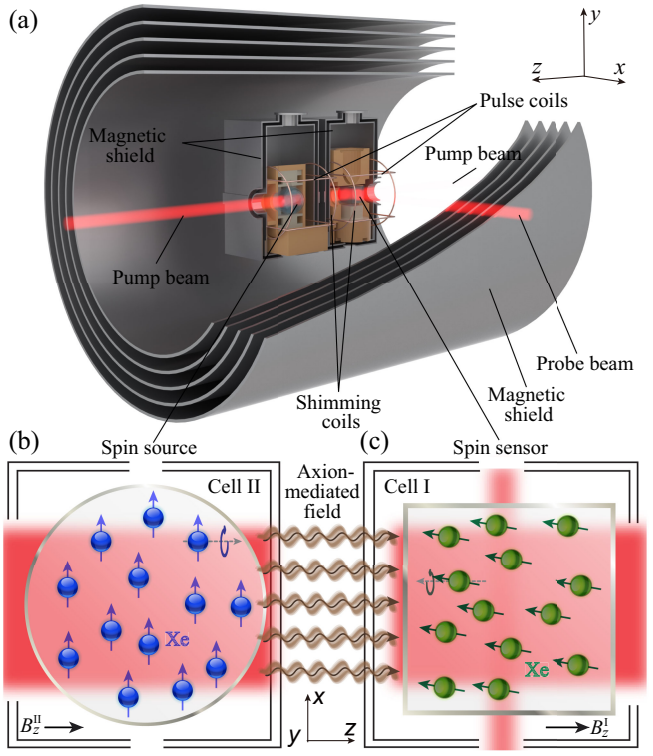

FIG. 1. Schematic of the experiment. Polarized ^{129}Xe spins in the source cell I are tilted into the x-y plane via a $\pi/2$ pulse and precess about the z axis, which generates free-decay pseudomagnetic fields on ^{129}Xe spins in the sensor cell II. (a) A three-dimensional layout. (b) A 795 nm pump beam tuned to the ^{87}Rb D1 transition delivers maximum 1.0 W of power to the source cell for optical pumping ^{87}Rb spins along $\hat{z}$. (c) In the sensor cell, ^{87}Rb spins are polarized with a circularly polarized beam of 795 nm D1 light and probed via optical rotation of a linearly polarized probe beam, which is detuned by 110 GHz to higher frequency from the D2 resonance.

$\mathbf{B}_p\hat{\boldsymbol{\sigma}}_{\text{I}} = -V_{\text{ps-ps}}/\mu_{\text{Xe}}$, where μ_{Xe} is the magnetic moment of ^{129}Xe nuclei. Figure 1(b) shows that free-decay pseudomagnetic fields are generated by precessing ^{129}Xe source spins in the x-y plane after a $\pi/2$ pulse

$$\mathbf{B}(t) = |\mathbf{B}_p|N_{\text{II}}^* e^{-t/T_{\text{II}}^*}[\cos(2\pi\nu_{\text{II}}t)\hat{x} + \sin(2\pi\nu_{\text{II}}t)\hat{y}], \quad (2)$$

where N_{II}^* is the total number of polarized ^{129}Xe spins, T_{II}^* is the effective coherence time, and ν_{II} is the ^{129}Xe Larmor frequency of source spins. The pseudomagnetic fields have both x and y components [64].

Magnetic amplification—Magnetic and pseudomagnetic fields $\mathbf{B}(t)$ collectively excite ensembles of polarized ^{129}Xe-sensor spins, as shown in Fig. 1(c). Because of Fermi-contact interactions [66–69], the transverse magnetization generated by these spins produces effective fields $\tilde{\mathbf{B}}(t)$ on ^{87}Rb spins [64],

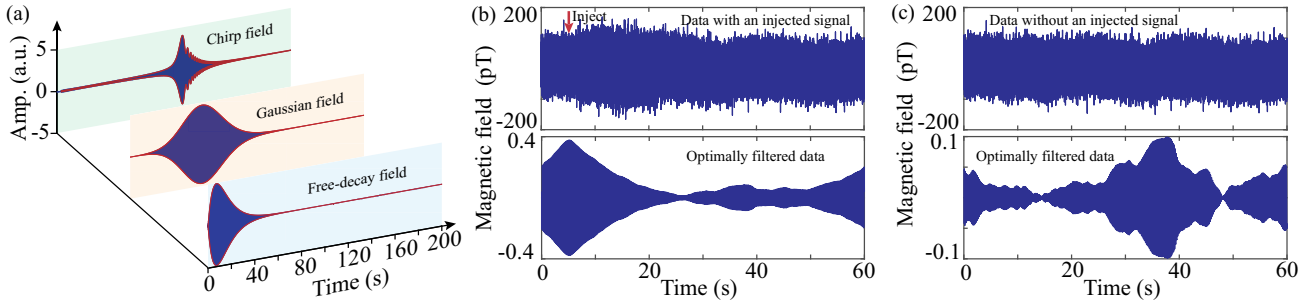

FIG. 2. Demonstration of the magnetic amplification and template filtering. (a) ^{129}Xe effective fields excited by various external fields. The envelope of experimental data (blue line) shows good agreement with the theoretical fit (red line). (b) Calibration of an injected signal with the template filter. The amplitude and arrival time of the injected signal can be exactly extracted (see main text). (c) Calibration of sensitivity.

$$\begin{bmatrix} \tilde{B}_x(\nu) \\ \tilde{B}_y(\nu) \end{bmatrix} \approx \eta \frac{1/T_{\mathrm{I}}^*}{i2\pi(\nu-\nu_{\mathrm{I}})+1/T_{\mathrm{I}}^*} \begin{bmatrix} 1 & 1 \\ -1 & 1 \end{bmatrix} \begin{bmatrix} B_x(\nu) \\ B_y(\nu) \end{bmatrix}, \quad (3)$$

where T_{I}^* is the effective coherence time (subscript I for sensor) and ν_{I} is the ^{129}Xe Larmor frequency. The ^{87}Rb magnetometer can simultaneously measure the external magnetic fields and the ^{129}Xe effective fields excited by external fields [64]. In the resonant case ($\nu \approx \nu_{\mathrm{I}}$), the amplitude of the ^{129}Xe effective fields $\tilde{\mathbf{B}}(\nu_{\mathrm{I}})$ is much greater than that of the external fields $\mathbf{B}(\nu_{\mathrm{I}})$, improving the sensitivity of the ^{87}Rb magnetometer. Such enhancement can be characterized with an amplification factor $\eta = |\tilde{\mathbf{B}}(\nu_{\mathrm{I}})|/|\mathbf{B}(\nu_{\mathrm{I}})| = 4\pi\kappa_0 M_{\mathrm{I}} P_{\mathrm{I}}^0 \gamma_n T_{\mathrm{I}}^*/3$ [64], where M_{I} is the ^{129}Xe maximum magnetization associated with full spin polarization, P_{I}^0 is the ^{129}Xe equilibrium polarization, and γ_n is the ^{129}Xe gyromagnetic ratio. The Fermi-contact enhancement factor κ_0 that characterizes the frequency shifts for Rb-^{129}Xe is measured to be 493 ± 31 [66–69]. Tailoring spin-monitoring experiments for high sensitivity using the effective fields was also demonstrated for K-He collisions [70], a system which was used to produce limits on pseudoscalar interactions [20] and Lorentz- and *CPT*-violating spin-spin interactions [71]. Recently, Rb-Xe effective fields have been used with large enhancements in the sensitivity to Xe spin for a transverse nuclear magnetic resonance gyroscope [72,73].

Equation (3) provides the ^{129}Xe effective fields in both frequency and time domains. Both x and y components of pseudomagnetic fields can induce rotating ^{129}Xe effective magnetic fields in the sensor. The resonant effective fields induced by free-decay pseudomagnetic fields in Eq. (2) are [64]

$$\tilde{B}_y(t) = 2\eta |\mathbf{B}_p| N_{\mathrm{II}}^* \frac{e^{-t/T_{\mathrm{I}}^*} - e^{-t/T_{\mathrm{II}}^*}}{1 - T_{\mathrm{I}}^*/T_{\mathrm{II}}^*} \cos(2\pi\nu_{\mathrm{I}} t + \phi), \quad (4)$$

where ϕ is the phase from rectangular $\pi/2$ pulses [64]. The response for $-\pi/2$ pulses includes a negative sign. The parameters of spin sensor, for example, $\nu_{\mathrm{I}} \approx 5.360$ Hz and $T_{\mathrm{I}}^* \approx 7.63$ s, are obtained by measuring the free-decay signal of the ^{129}Xe spins. $\eta \approx 145$ is calibrated by applying auxiliary continuous fields, one at the resonance frequency ν_{I} and the other—far from resonance—at 70 Hz. Subsequently, Eq. (4) is experimentally verified by applying a synthetic "free-decay" resonant field with a strength of $\approx$10.0 pT and a coherence time of $T_{\mathrm{II}}^* \approx 7.04$ s along y [see Fig. 2(a)].

To demonstrate the characteristics of noble-gas magnetic amplification, Fig. 2(a) also shows the experimental response to a Gaussian field and a chirp field with linearly modulated frequency. The theoretical fitting based on Eq. (3) is in good accordance with experimental results [64]. More examples are presented in Supplemental Material [64].

We have significantly enhanced the sensitivity to weak fields in our sensor cell by integrating two experimental techniques. First, resonant interactions between pseudomagnetic fields and the sensor's spins maximize the ^{129}Xe transverse polarization in the sensor cell for resonant source fields. Second, the ^{129}Xe transverse polarization in the sensor cell via Rb-^{129}Xe Fermi-contact interactions substantially amplifies the detected ^{129}Xe signal [66–69]. To realize our full sensitivity gain, a meticulous selection of several key physical parameters $\{\kappa_0, M_{\mathrm{I}}, P_{\mathrm{I}}^0, T_{\mathrm{I}}^*\}$ is required (see Supplemental Material [64] for details). This combined signal enhancement can be considered an effective amplification of the weak fields, which we refer to as "magnetic amplification," and is linear for the weak fields considered here.

Noise reduction using a signal template—The main objective of our experiment is to extract the unknown amplitude of the sought-after signal with the known template [see Eq. (4)] by maximizing signal-to-noise ratio. To achieve this, we use a template filtering technique akin

to that used by the Laser Interferometer Gravitational Wave Observatory in gravitational wave detection [74]. The template filter $\Omega(\nu) = \alpha \tilde{B}_y^*(\nu)/S_n(\nu)$ is designed based on the power spectral density of noise $S_n(\nu)$ including color noise and technical noise peak [75] and functional form of $\tilde{B}_y$, where α is the normalization factor. The extracted field $B_y^{\mathrm{exp}}(t)$ is [64]

$$B_y^{\mathrm{exp}}(t) = \int_{-\infty}^{\infty} e^{i2\pi\nu t}\Omega(\nu)\tilde{B}_y(\nu)d\nu. \tag{5}$$

The signal contributes coherently to the cross-correlation with the template, while the noise contributes incoherently and thus is reduced relative to the signal. The filter is proven to be the optimal linear filter for maximizing the signal-to-noise ratio. Additionally, while not relevant for the present exotic-force search, template filtering can be used to extract signals with unknown arrival times, which is difficult to achieve using conventional spectral analysis [64]. For white noise in our case, the template filter is reduced to the matched filter.

The parameters of template are calibrated by a series of experiments [64]. Former experiments calibrate parameters of the sensor cell (ν_{I}, η, and T_{I}^*) and the rest of the source cell (N_{II}^*, T_{II}^*, ν_{II}, and ϕ) are calibrated using the atomic magnetometer itself. A small-angle pulse is applied to measure the free-decay signal through the ^{87}Rb magnetometer, and the coherence time T_{II}^* and the Larmor frequency ν_{II} can be directly obtained by fitting the signal. To measure the polarization, an auxiliary continuous field is applied to obtain the conversion coefficient from magnetic field to voltage. Then the amplitude of the decay signal is transformed into the field strength and compared to the effective magnetic field of 3 amg of fully polarized ^{129}Xe to obtain the polarization [66–69].

With the calibrated template, we apply the template filter to the data with or without an injected signal. The injected signal with the same template and a field strength of ≈0.4 pT arrives at unknown times. As shown in Fig. 2(b), the injected signal is almost hidden inside the noise because of the 50-Hz power line interference. With a remarkable improvement of the signal-to-noise ratio, the strength and arrival time (5 s) is exactly extracted. We further demonstrate the improved magnetic sensitivity with template sensing for a 60-s single-shot experiment. Figure 2(c) shows a time-domain sensitivity of 28.1 pT for the ^{87}Rb magnetometer. A further improvement is achieved by applying the template filter. The amplitude of the filtered noise at 5 s represents the extracted field strength for a single-shot experiment. By applying the template filter to 1000 such experiments, the standard deviation of extracted strength corresponds to a sensitivity of ≈30 fT, which improves the sensitivity by at least 2 orders of magnitude.

Search experiments and data analysis—The ^{129}Xe response $\tilde{B}_y(\nu)$ can be maximized by optimizing the operation parameters of the spin source such as temperature, pumping power, pressure, etc. We first fix the pump power at 1.0 W, change the temperature to obtain number of tilted polarized ^{129}Xe N_{II}^* and coherence time T_{II}^*. It is found that the polarization increases but the relaxation time reduces with increasing temperature, as shown in Fig. 3(a). The amplitude of $\tilde{B}_y(\nu)$ is calculated and reaches maximum around 105 °C, as shown in Fig. 3(b). Subsequently, we set the operation temperature at 105 °C and change the pumping power. Figure 3(c) shows that the polarization increases but the relaxation time reduces with the increasing power. The decrease of the coherence time can be caused by the gradient field of nonuniform ^{87}Rb polarization along the radial direction, because of the inhomogeneity of light intensity of pump beam and edge of the vapor cell that is not illuminated. The amplitude of $\tilde{B}_y(\nu)$ shows marginal increase up to the highest power used of 1.0 W, as shown in Fig. 3(d). At 105 °C and 1.0 W, the experimental parameters are $\nu_{\mathrm{II}} \approx 5.360$ Hz, $N_{\mathrm{II}}^* \approx 4.0 \times 10^{18}$, and $T_{\mathrm{II}}^* \approx 7.04$ s.

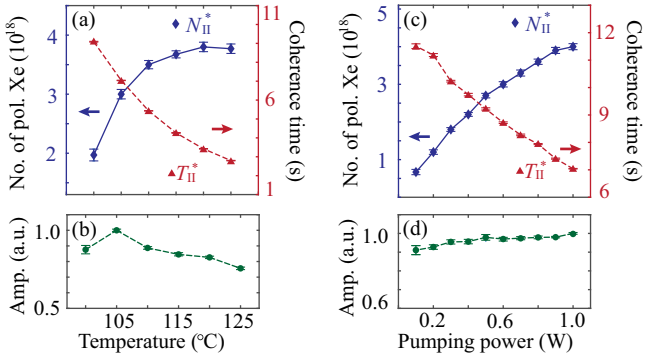

FIG. 3. Calibration of spin-source parameters and optimization of them for maximizing $\tilde{B}_y$. (a) The coherence time (red line) is reduced but the polarization (blue line) is increased with increasing temperature. (b) The amplitude of $\tilde{B}_y(\nu)$ reaches maximum at 105 °C. (c) The coherence time (red line) is reduced but the polarization (blue line) is increased with increasing pumping power. (d) The amplitude of $\tilde{B}_y(\nu)$ shows marginal increase up to the maximum available laser power (1.0 W) emitted into the source cell.

To induce the pseudomagnetic fields, $\pm\pi/2$ pulses are alternately applied every 60 s to initiate a single-shot experiment. Subsequently, the single-shot experiment is repeated 1200 times over a 20-h data collection period to generate a single dataset (see Supplemental Material [64] for details). Then the sensitivity of the spin sensor is optimized and recorded. The experimental conditions (e.g., temperature, pump power, laser frequency) of the spin source are monitored and adjusted to maintain stable operation. The data collection is repeated 36 times over a 720-h data collection period, yielding a total of 36 datasets. The raw spin-sensor data are segmented into ≈60 s segments based on the pulse sequence, because the response of ^{129}Xe spins spans approximately 60 s [see Eq. (4)], as shown

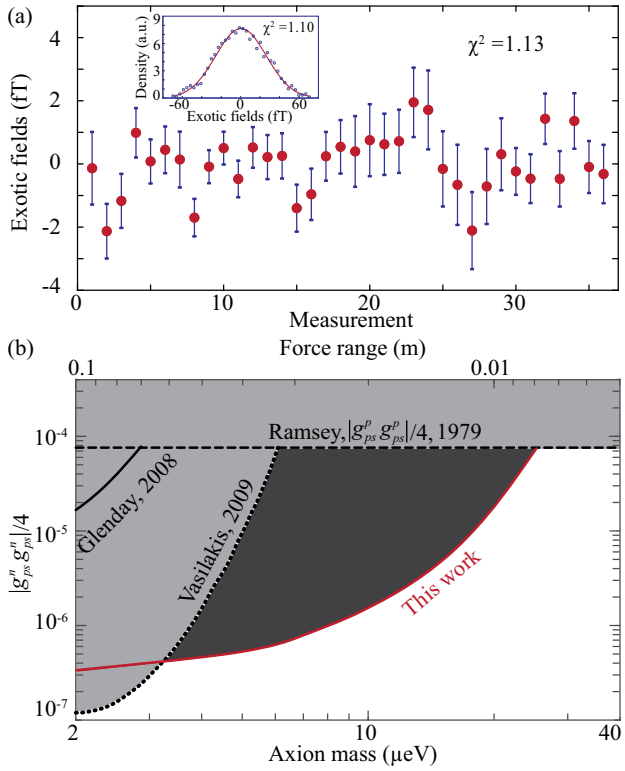

FIG. 4. Experimental results. (a) Each point represents the average and statistical error of exotic fields for a 20-h dataset. Inset: histogram of a 20-h dataset with a Gaussian fit in red line. (b) Constraints on $|g^n_{\rm ps} g^n_{\rm ps}|/4$. The black line represents the results from previous experiments of Ramsey [56], Glenday *et al.* [21], and Vasilakis *et al.* [20]. The red line represents the new constraints, improving former constraints by a factor about 118 at 6.04 μeV and 50 at 10 μeV.

in Fig. 2(a). The normalized template filter is then applied to each segment. The first data point of the resulting filtered signal is extracted as the measured exotic field. A typical distribution of the exotic fields deduced from 20-h data shows a standard deviation of ≈30 fT, as shown in the inset of Fig. 4(a).

Using all the 720 h of data, the exotic fields are measured to be $(-86 \pm 140_{\rm stat})$ aT between the two separated neutron ensembles, which is less than 10^{-5} of their magnetic interactions on a length scale of 60 mm. The spurious magnetic fields generated by the polarized ^{129}Xe spins and magnetic pulses are suppressed by the magnetic screening effect originating from the attenuation due to distance and the use of magnetic shields. The screening factor is over 10^{10} through cross-check from theoretical calculations, numerical simulations, and experimental calibrations [64,76]. The ^{129}Xe classical dipole fields are reduced to ≈0.2 aT and magnetic pulses are reduced to 50 aT with 20 ms duration, both of which are negligible.

We include possible systematic errors in the calibration that come from variations in number of polarized ^{129}Xe $N^*_{\rm II}$, coherence time $T^*_{\rm I}$ and $T^*_{\rm II}$, position, resonance frequency $\nu_{\rm II}$, the phase ϕ, and the amplification factor η. By measuring all these factors and combining the corresponding uncertainties in quadrature, which are assumed to be independent of each other, the total uncertainty in the systematic error is ≈45 aT [64]. We thus find no evidence for the axions and quote the final total coupling strength $|g^n_{\rm ps} g^n_{\rm ps}|/4$ as $(2.0 \pm 3.2_{\rm stat} \pm 1.1_{\rm sys}) \times 10^{-7}$ at $m_a = 4.94$ μeV.

Figure 4(b) shows the obtained constraints together with those from previous experiments [20,21,56]. The red line represents the new constraints with 1σ limit, part of which reaches into the unexplored parameter space within the axion window. The dashed line represents the first constraint of exotic spin-spin interactions derived by Ramsey [56]. Then the maser [21] (the solid line) and the comagnetometer [20] (the dotted line) experiment placed constraints on $|g^n_{\rm ps} g^n_{\rm ps}|/4$ outside the axion window. For the mass range from 3.2 to 24.3 μeV, we set the most stringent constraints on $|g^n_{\rm ps} g^n_{\rm ps}|/4$, improving previous constraints by a factor about 118 at 6.04 μeV and 50 at 10 μeV within the axion window. We can also place constraints on proton-proton pseudoscalar couplings $|g^p_{\rm ps} g^p_{\rm ps}|/4$, which improve on those from Ramsey's measurements [20,56] by up to 16-fold.

Conclusion and discussion—In this Letter, we report the magnetic amplification and template filtering and apply them to search for axion-mediated spin-dependent interactions. These techniques extract the template signal with a spin amplification of at least 2 orders of magnitude and a maximum signal-to-noise ratio. Using our technique, new constraints on pseudoscalar couplings are set within the axion window.

Our technique can be applied to probe axion dark matter directly coupling to the ^{129}Xe neutron spins (no spin source is needed). For "axion wind," axions generate oscillating exotic fields proportional to the coupling constant $g_{\rm aNN}$ [77]. The spin sensor is sensitive to the axions within a narrow bandwidth centered at 5.36 Hz. The current sensitivity $g_{\rm aNN} \approx 10^{-9}$ GeV^{-1} could exceed the astrophysical limits [59,60] in a frequency range of ≈5.33–5.39 Hz. Our technique can also be employed to search for topological defect dark matter consisting of axions [57]. The pseudomagnetic fields of it are similar to magnetic pulses, which could induce free-decay ^{129}Xe effective magnetic fields. The functional form of these free-decay fields is the template for topological defect dark matter searches. By combining the magnetic amplification and template filtering, the 720-h data correspond to a sensitivity to the coupling of topological defect dark matter and nuclear spins ≈10^{-10} GeV^{-1}, exceeding the astrophysical limit [59,60] with the mass range of 10^{-10}–10^{-7} eV and a fixed symmetry-breaking scale ≈10^{11} eV [57].

Our technique could also be used to constrain bursts of axion fields produced from binary black holes [58]. Axion

bursts lag behind the emitted gravitational waves that act as triggers for detection. Assuming isotropic propagation of exotic fields, the field strength decreases with the increasing distance from its source, reducing the sensitivity to the coupling strength. Using the functional form of axions bursts in Ref. [57] as template, our sensor could achieve an energy resolution of 10^{-22} eV/Hz$^{1/2}$. For the prior astrophysical limits on linear coupling $\approx 10^8$ GeV and quadratic coupling 10^4 GeV [58], our sensor could have an astrophysical reach of 10^8 light years.

Acknowledgments—We thank Victor Flambaum, Yevgeny Stadnik, Yifan Chen, and Pavel Fadeev for valuable discussions. This work was supported by the Innovation Program for Quantum Science and Technology (Grant No. 2021ZD0303205), National Natural Science Foundation of China (Grants No. T2388102, No. 11927811, No. 12150014, No. 12274395, No. 12261160569, No. 12404341), Youth Innovation Promotion Association (Grant No. 2023474), and China Postdoctoral Science Foundation (BX20240352, 2024M753082) and the Fundamental Research Funds for the Central Universities. This work was also supported by the Cluster of Excellence "Precision Physics, Fundamental Interactions, and Structure of Matter" (PRISMA+EXC 2118/1) funded by the German Research Foundation (DFG) within the German Excellence Strategy (Project ID No. 39083149).

[1] R. D. Peccei and H. R. Quinn, *CP* conservation in the presence of pseudoparticles, Phys. Rev. Lett. **38**, 1440 (1977).
[2] F. Wilczek, Problem of strong P and T invariance in the presence of instantons, Phys. Rev. Lett. **40**, 279 (1978).
[3] J. E. Kim and G. Carosi, Axions and the strong *CP* problem, Rev. Mod. Phys. **82**, 557 (2010).
[4] Z. Berezhiani and M. Y. Khlopov, Cosmology of spontaneously broken gauge family symmetry with axion solution of strong *CP*-problem, Z. Phys. C **49**, 73 (1991).
[5] M. Safronova *et al.*, Search for new physics with atoms and molecules, Rev. Mod. Phys. **90**, 025008 (2018).
[6] D. DeMille, J. M. Doyle, and A. O. Sushkov, Probing the frontiers of particle physics with tabletop-scale experiments, Science **357**, 990 (2017).
[7] P. W. Graham and S. Rajendran, New observables for direct detection of axion dark matter, Phys. Rev. D **88**, 035023 (2013).
[8] M. Pospelov *et al.*, Detecting domain walls of axionlike models using terrestrial experiments, Phys. Rev. Lett. **110**, 021803 (2013).
[9] S. Borsanyi *et al.*, Calculation of the axion mass based on high-temperature lattice quantum chromodynamics, Nature (London) **539**, 69 (2016).
[10] G. Ballesteros, J. Redondo, A. Ringwald, and C. Tamarit, Unifying inflation with the axion, dark matter, baryogenesis, and the seesaw mechanism, Phys. Rev. Lett. **118**, 071802 (2017).
[11] V. B. Klaer and G. D. Moore, The dark-matter axion mass, J. Cosmol. Astropart. Phys. 11 (2017) 049.
[12] M. S. Turner, Windows on the axion, Phys. Rep. **197**, 67 (1990).
[13] A. Youdin, D. Krause Jr, K. Jagannathan, L. Hunter, and S. Lamoreaux, Limits on spin-mass couplings within the axion window, Phys. Rev. Lett. **77**, 2170 (1996).
[14] A. Arvanitaki and A. A. Geraci, Resonantly detecting axion-mediated forces with nuclear magnetic resonance, Phys. Rev. Lett. **113**, 161801 (2014).
[15] Q. Yang, Probe dark matter axions using the hyperfine structure splitting of hydrogen atoms, arXiv:192.11472.
[16] M. Jiang, H. Su, A. Garcon, X. Peng, and D. Budker, Search for axion-like dark matter with spin-based amplifiers, Nat. Phys. **17**, 1402 (2021).
[17] G. G. Raffelt, Axion constraints from white dwarf cooling times, Phys. Lett. B **166**, 402 (1986).
[18] A. Ayala, I. Domínguez, M. Giannotti, A. Mirizzi, and O. Straniero, Revisiting the bound on axion-photon coupling from globular clusters, Phys. Rev. Lett. **113**, 191302 (2014).
[19] A. Garcon *et al.*, Constraints on bosonic dark matter from ultralow-field nuclear magnetic resonance, Sci. Adv. **5**, eaax4539 (2019).
[20] G. Vasilakis, J. Brown, T. Kornack, and M. Romalis, Limits on new long range nuclear spin-dependent forces set with a K-^{3}He comagnetometer, Phys. Rev. Lett. **103**, 261801 (2009).
[21] A. G. Glenday, C. E. Cramer, D. F. Phillips, and R. L. Walsworth, Limits on anomalous spin-spin couplings between neutrons, Phys. Rev. Lett. **101**, 261801 (2008).
[22] T. Braine *et al.*, Extended search for the invisible axion with the axion dark matter experiment, Phys. Rev. Lett. **124**, 101303 (2020).
[23] J. Lee, M. Lisanti, W. A. Terrano, and M. Romalis, Laboratory constraints on the neutron-spin coupling of feV-scale axions, Phys. Rev. X **13**, 011050 (2023).
[24] P. Gondolo and G. G. Raffelt, Solar neutrino limit on axions and keV-mass bosons, Phys. Rev. D **79**, 107301 (2009).
[25] Y. Wang *et al.*, Limits on axions and axionlike particles within the axion window using a spin-based amplifier, Phys. Rev. Lett. **129**, 051801 (2022).
[26] K. M. Backes *et al.*, A quantum enhanced search for dark matter axions, Nature (London) **590**, 238 (2021).
[27] CAST Collaboration, New CAST limit on the axion–photon interaction, Nat. Phys. **13**, 584 (2017).
[28] B. T. McAllister *et al.*, The ORGAN experiment: An axion haloscope above 15 GHz, Phys. Dark Universe **18**, 67 (2017).
[29] A. Quiskamp *et al.*, Direct search for dark matter axions excluding ALP cogenesis in the 63- to 67-μeV range with the organ experiment, Sci. Adv. **8**, eabq3765 (2022).
[30] P. Brun *et al.*, A new experimental approach to probe QCD axion dark matter in the mass range above 40 μeV, Eur. Phys. J. C **79**, 1 (2019).
[31] G. Rybka *et al.*, Search for dark matter axions with the orpheus experiment, Phys. Rev. D **91**, 011701(R) (2015).

[32] N. Aggarwal *et al.*, Characterization of magnetic field noise in the ARIADNE source mass rotor, Phys. Rev. Res. **4**, 013090 (2022).

[33] S. Weinberg, A new light boson?, Phys. Rev. Lett. **40**, 223 (1978).

[34] B. A. Dobrescu and I. Mocioiu, Spin-dependent macroscopic forces from new particle exchange, J. High Energy Phys. 11 (2006) 005.

[35] J. Moody and F. Wilczek, New macroscopic forces?, Phys. Rev. D **30**, 130 (1984).

[36] P. Fadeev *et al.*, Revisiting spin-dependent forces mediated by new bosons: Potentials in the coordinate-space representation for macroscopic-and atomic-scale experiments, Phys. Rev. A **99**, 022113 (2019).

[37] X. Rong *et al.*, Searching for an exotic spin-dependent interaction with a single electron-spin quantum sensor, Nat. Commun. **9**, 1 (2018).

[38] W. Terrano, E. Adelberger, J. Lee, and B. Heckel, Short-range, spin-dependent interactions of electrons: A probe for exotic pseudo-Goldstone bosons, Phys. Rev. Lett. **115**, 201801 (2015).

[39] B. R. Heckel *et al.*, Preferred-frame and *CP*-violation tests with polarized electrons, Phys. Rev. D **78**, 092006 (2008).

[40] P.-H. Chu *et al.*, Laboratory search for spin-dependent short-range force from axionlike particles using optically polarized ^{3}He gas, Phys. Rev. D **87**, 011105 (2013).

[41] M. Bulatowicz *et al.*, Laboratory search for a long-range *T*-odd, *P*-odd interaction from axionlike particles using dual-species nuclear magnetic resonance with polarized ^{129}Xe and ^{131}Xe gas, Phys. Rev. Lett. **111**, 102001 (2013).

[42] Y. Stadnik, V. Dzuba, and V. Flambaum, Improved limits on axionlike-particle-mediated *P*, *T*-violating interactions between electrons and nucleons from electric dipole moments of atoms and molecules, Phys. Rev. Lett. **120**, 013202 (2018).

[43] H. Yan and W. Snow, New limit on possible long-range parity-odd interactions of the neutron from neutron-spin rotation in liquid ^{4}He, Phys. Rev. Lett. **110**, 082003 (2013).

[44] L. Wu, K. Zhang, M. Peng, J. Gong, and H. Yan, New limits on exotic spin-dependent interactions at astronomical distances, Phys. Rev. Lett. **131**, 091002 (2023).

[45] P. Fadeev, F. Ficek, M. G. Kozlov, D. Budker, and V. V. Flambaum, Pseudovector and pseudoscalar spin-dependent interactions in atoms, Phys. Rev. A **105**, 022812 (2022).

[46] M. Ledbetter, M. V. Romalis, and D. J. Kimball, Constraints on short-range spin-dependent interactions from scalar spin-spin coupling in deuterated molecular hydrogen, Phys. Rev. Lett. **110**, 040402 (2013).

[47] S. Kotler, R. Ozeri, and D. F. J. Kimball, Constraints on exotic dipole-dipole couplings between electrons at the micrometer scale, Phys. Rev. Lett. **115**, 081801 (2015).

[48] F. Ficek *et al.*, Constraints on exotic spin-dependent interactions between electrons from helium fine-structure spectroscopy, Phys. Rev. A **95**, 032505 (2017).

[49] B. Heckel, W. Terrano, and E. Adelberger, Limits on exotic long-range spin-spin interactions of electrons, Phys. Rev. Lett. **111**, 151802 (2013).

[50] A. Almasi, J. Lee, H. Winarto, M. Smiciklas, and M. V. Romalis, New limits on anomalous spin-spin interactions, Phys. Rev. Lett. **125**, 201802 (2020).

[51] W. Ji *et al.*, New experimental limits on exotic spin-spin-velocity-dependent interactions by using $SmCo_5$ spin sources, Phys. Rev. Lett. **121**, 261803 (2018).

[52] L. Hunter, J. Gordon, S. Peck, D. Ang, and J.-F. Lin, Using the Earth as a polarized electron source to search for long-range spin-spin interactions, Science **339**, 928 (2013).

[53] J. Ding *et al.*, Constraints on the velocity and spin dependent exotic interaction at the micrometer range, Phys. Rev. Lett. **124**, 161801 (2020).

[54] J. E. Kim, Light pseudoscalars, particle physics and cosmology, Phys. Rep. **150**, 1 (1987).

[55] R. T. Hammond, Torsion gravity, Rep. Prog. Phys. **65**, 599 (2002).

[56] N. F. Ramsey, The tensor force between two protons at long range, Physica (Amsterdam) **96A**, 285 (1979).

[57] S. Afach *et al.*, Search for topological defect dark matter using the global network of optical magnetometers for exotic physics searches (GNOME), Nat. Phys. **17**, 1396 (2021).

[58] C. Dailey *et al.*, Quantum sensor networks as exotic field telescopes for multi-messenger astronomy, Nat. Astron. **5**, 150 (2021).

[59] G. G. Raffelt, Astrophysical axion bounds, in *Axions: Theory, Cosmology, and Experimental Searches* (Springer, New York, 2008), pp. 51–71.

[60] J. H. Chang, R. Essig, and S. D. McDermott, Supernova 1987A constraints on sub-GeV dark sectors, millicharged particles, the QCD axion, and an axion-like particle, J. High Energy Phys. 09 (2018) 051.

[61] T. G. Walker and W. Happer, Spin-exchange optical pumping of noble-gas nuclei, Rev. Mod. Phys. **69**, 629 (1997).

[62] T. R. Gentile, P. Nacher, B. Saam, and T. Walker, Optically polarized ^{3}He, Rev. Mod. Phys. **89**, 045004 (2017).

[63] D. J. Kimball, Nuclear spin content and constraints on exotic spin-dependent couplings, New J. Phys. **17**, 073008 (2015).

[64] See Supplemental Materials at http://link.aps.org/supplemental/10.1103/PhysRevLett.133.191801, which includes Ref. [65], for details of experimental setup, noble-gas magnetic amplification, template filtering, and data analysis.

[65] M. V. Romalis, E. Miron, and G. D. Cates, Pressure broadening of Rb D_1 and D_2 lines by ^{3}He, ^{4}He, N_2, and Xe: Line cores and near wings, Phys. Rev. A **56**, 4569 (1997).

[66] Z. Ma, E. Sorte, and B. Saam, Collisional ^{3}He and ^{129}Xe frequency shifts in Rb–noble-gas mixtures, Phys. Rev. Lett. **106**, 193005 (2011).

[67] X. Liu, H. Luo, T. Qu, K. Yang, and Z. Ding, Measuring the spin polarization of alkali-metal atoms using nuclear magnetic resonance frequency shifts of noble gases, AIP Adv. **5**, 107119 (2015).

[68] A. Nahlawi, Z. Ma, M. Conradi, and B. Saam, High-precision determination of the frequency-shift enhancement factor in Rb-^{129}Xe, Phys. Rev. A **100**, 053415 (2019).

[69] S. Schaefer *et al.*, Frequency shifts of the magnetic-resonance spectrum of mixtures of nuclear spin-polarized noble gases and vapors of spin-polarized alkali-metal atoms, Phys. Rev. A **39**, 5613 (1989).

[70] T. Kornack and M. Romalis, Dynamics of two overlapping spin ensembles interacting by spin exchange, Phys. Rev. Lett. **89**, 253002 (2002).

[71] J. M. Brown, S. J. Smullin, T. W. Kornack, and M. V. Romalis, New limit on lorentz-and *CPT*-violating neutron spin interactions, Phys. Rev. Lett. **105**, 151604 (2010).

[72] S. S. Sorensen and T. G. Walker, Combined polarization/magnetic modulation of a transverse NMR gyroscope, Sensors **23**, 4649 (2023).

[73] D. A. Thrasher, S. S. Sorensen, and T. G. Walker, Dual-species synchronous spin-exchange optical pumping, arXiv:1912.04991.

[74] B. Abbott *et al.*, Analysis of first LIGO science data for stochastic gravitational waves, Phys. Rev. D **69**, 122004 (2004).

[75] L. A. Wainstein and V. Zubakov, *Extraction of Signals from Noise* (Dover Publications, Inc., New York, 1970).

[76] T. Sumner, J. Pendlebury, and K. Smith, Convectional magnetic shielding, J. Phys. D **20**, 1095 (1987).

[77] D. Budker, P. W. Graham, M. Ledbetter, S. Rajendran, and A. O. Sushkov, Proposal for a cosmic axion spin precession experiment (CASPEr), Phys. Rev. X **4**, 021030 (2014).